Journal of Electroceramics, 13, 345–352, 2004

Effect of Strain Gradation on Luminescence and Electronic Properties of Pulsed Laser Deposited Zinc Oxide Thin Films

A.C. RASTOGI,[1,*] S.B DESU,[1] P. BHATTACHARYA[2] & R.S. KATIYAR[2]
[1]*Department of Electrical & Computer Engineering, University of Massachusetts, Amherst, MA 01003*
[2]*Department of Physics, University of Puerto Rico, Rio Piedras, P.R. 00931*

Submitted March 3, 2003; Revised May 11, 2004; Accepted May 12, 2004

Abstract. ZnO thin films were grown by ablation of a ZnO ceramic target using pulsed excimer laser (KrF) under 1 mTorr oxygen partial pressure over (0001) α-Al_2O_3 substrates held at 750°C. Highly *c*-axis oriented (0002) ZnO films with visible range optical transparency over 80% were obtained. Inhomogeneous distribution of strain in the film growth direction was studied by line shape analysis of X-ray diffraction and broad luminescence features centered on near band edge transition at 3.3 eV. Strain in the film adversely affects optical gain and excitonic threshold of UV emission. Post-growth oxygen annealing of films at 850°C for 1 h reduces strain and associated defects at ZnO film interface with (0001) Al_2O_3 substrate. FWHM of X-ray rocking curves show corresponding lowering from 12.5 arc min to 9.0 arc min signifying improved ZnO crystal quality. ω-rocking curves show line features with two superimposed peaks belonging to interfacial layer and bulk ZnO film. Graded strain in ZnO film is related to differently oriented interfacial layer formed at inception stage of film growth. Decrease in conductivity of annealed ZnO films show that O_2-vacancies are primary defects. Formation of strain free (0002) oriented optical quality ZnO films based on combined process of growth in low O_2 pressure and post growth anneal at high O_2 pressure is proposed for UV-optoelectronic applications.

Keywords: epitaxial ZnO films, pulsed laser deposition, ultraviolet light emission, luminescence, wide band gap

1. Introduction

Zinc oxide exhibits wide ranging technological applications in acousto-optical devices, gas selective chemical sensors, conducting transparent electrodes for solar cells and displays etc. These applications exploit its unique combined piezoelectric, electrical and optical properties, which are attainable with polycrystalline films. Current research interest in ZnO epitaxial films stems from its potential applications in ultraviolet optoelectronics. ZnO properties, wide (3.37 eV) direct band gap, large (60 meV) excitonic binding energy, high temperature stability and chemical inertness are attractive for fabrication of such devices. Recently, spontaneous UV emission [1], excitonic lasing [2] and biexciton emission [3] have been demonstrated in epitaxial ZnO films which has stimulated considerable interest in epitaxial growth of ZnO films. Although a number of growth techniques have been employed to form ZnO films, chemical vapor deposition [4], pulsed laser deposition PLD [5, 6] and free radical, laser or plasma assisted molecular beam epitaxy MBE [7–9] are widely studied to form high quality single crystal ZnO films useful for devices. ZnO epitaxial films are generally grown over *c*-plane sapphire (α-Al_2O_3) substrates. Large lattice mismatch ($\sim$16.8%) and difference in thermal expansion coefficients between ZnO and α-Al_2O_3 could possibly cause inclusion of strain and defects in films during growth. These affect ZnO properties, particularly excitonic binding energy, surface microstructure and crystalline structure. Fabrication of ZnO/α-Al_2O_3 heterostructures with low excitonic lasing threshold and high optical gain are important for optical devices. It is relevant to investigate strain effects in ZnO films Deposition of ZnO films at lower temperature as in PLD technique therefore appears attractive. In this paper we describe growth of highly oriented ZnO films by pulsed laser ablation

*To whom all correspondence should be addressed.

technique and effect of strain in such films on photoluminescence properties.

2. Experimental

ZnO thin films were grown by pulsed laser ablation technique over *c*-axis oriented sapphire (α-Al_2O_3 crystals) substrates. Ceramic target of 25 mm diameter was prepared by conventional powder processing route using 99.99% pure ZnO powder. Laser ablation was carried out using KrF (248 nm) excimer laser with pulse energy density ∼2–2.5 J/cm^2 at 10 Hz pulse repetition rate. Prior to film growth, deposition chamber was evacuated down to 0.0 1 mTorr and then backfilled by introduction of O_2 to 1 mTorr oxygen pressure. ZnO films were deposited over double side polished α-Al_2O_3 crystal substrates heated to 750°C and kept at ∼5 cm distance from ZnO target. Film thickness ranged between 300–350 nm as measured using Alpha 100 step-scan TENCOR instrument. ZnO films were annealed at constant temperature between 800–900°C for 1 h each in standard furnace under continuous oxygen flow. Crystal structure of ZnO films was determined by conventional X-ray θ–2θ diffraction scans using CuK_α radiation in a Siemens D5000 diffractometer. ω-scan rocking curves were obtained on a Bede QC1 diffractometer. Full width at half maximum (FWHM) of rocking curves yield information on orientation distribution of the lattice planes with a definite lattice parameter to characterize ZnO film growth over substrates. Measurements of electrical resistivity and mobility of ZnO thin films were done in Van der Pauw configuration using sputtered gold film contacts. Irradiating ZnO films by 325 nm emission line of a 20 mW continuous wave He-Cd laser excited the photoluminescence (PL) spectra. Emission from ZnO films was dispersed by a 600 mm focal length monochromator equipped with double 1200 lines/mm grating blazed at 400 nm. PL emission was detected using a standard GaAs photomultiplier tube and photon counting system and recorded at 296 K with 0.2 nm resolution.

3. Results and Discussion

3.1. X-ray Diffraction Studies

X-ray θ–2θ diffraction scans along the growth direction of as deposited and O_2-annealed ZnO films formed over *c*-plane sapphire (α-Al_2O_3) substrates are shown in Fig. 1. High intensity (0002) ZnO reflection along with its lower intensity (0004) harmonic from hexagonal wurzite structure is observed. FWHM of (0002) reflection is ∼0.94° which shows highly *c*-axis oriented ZnO film growth. Other strong diffraction line is from (0006) plane of single crystal substrate. Additional information about the structural properties of oriented ZnO films is obtained by thin film strains. For this analysis, distance between the lattice planes d_{hkl} of epitaxial ZnO films was treated as an internal strain gauge [10]. Strain $\varepsilon_\perp$ in the direction of diffraction vector $\vec{\ell}$ normal to the planes with spacing d_{hkl} is defined as $\varepsilon_\perp \approx (d_{hkl} - d_B)/d_B$, where d_B is lattice spacing corresponding to the bulk crystal in unstressed form. In the present case, as highly *c*-axis oriented ZnO films are formed; there are no diffraction peaks in X-ray diffraction pattern to identify in-plane lattice strain. Determination of strain in ZnO films was made using d_{hkl} values based only on (0002) reflection. Out of plane lattice parameter changes with annealing conditions resulting in reduction of *c*-direction strain from 3.3×10^{-2} to 1.9×10^{-3} as shown in Fig. 2. Analogous to earlier inferences drawn from studies on GaN, in ZnO with

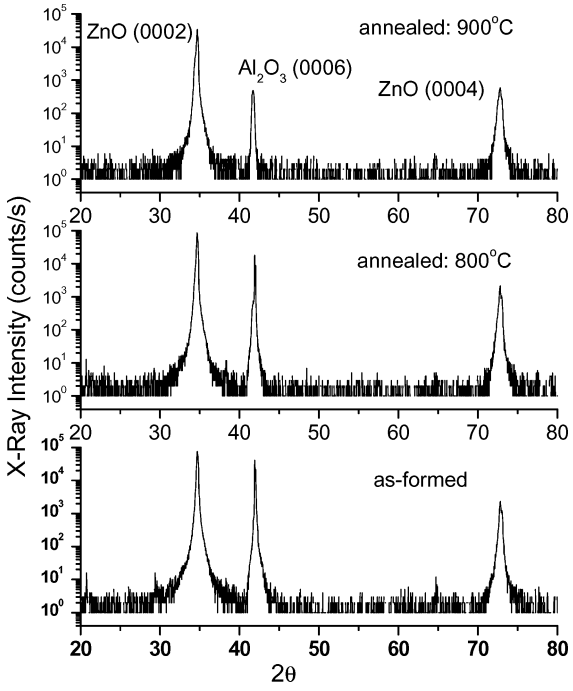

Fig. 1. X-ray diffraction pattern of as-deposited and O_2-annealed ZnO films showing *c*-axis orientation.

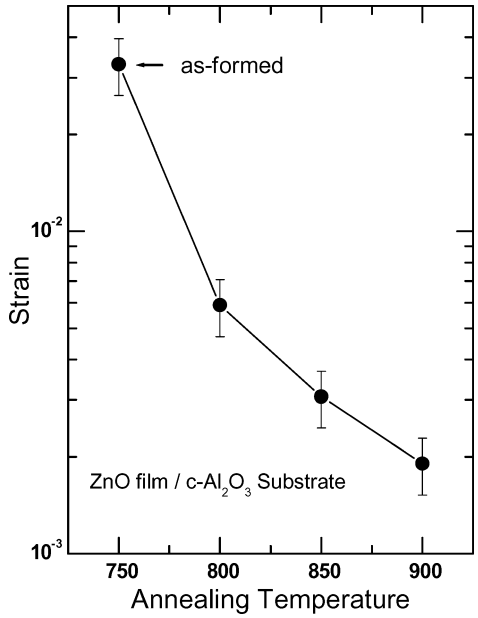

Fig. 2. Reduction in strain in ZnO films by oxygen annealing at different temperatures.

hexagonal structure, *c*-axis strain proportionally acts on generation of biaxial compressive film stress parallel to the direction of the film plane [11]. Reason for elastic lattice strain in ZnO film is ∼16.8% lattice mismatch between (0001) α-Al_2O_3 substrate and (0002) ZnO film planes. Thermal origin of strain is derived from differences in thermal expansion coefficients.

X-ray ω-rocking curve of (0002) reflection from as-deposited ZnO film has asymmetrical line shape as shown in Fig. 3(a). Rocking curves of several similarly deposited films are also found identical in nature. Fitting Gaussian line shape to ω-peak profile reveals that observed rocking curve is superposition of two distinct peaks. An intense sharp peak with FWHM, ∼11.2 arc min and other a broader low intensity peak with FWHM ∼13.5 arc min. Narrower peak of ω-rocking curve due to coherent diffraction originates from region of film with high crystalline perfection. High intensity of this peak indicates that bulk of film has oriented crystalline structure with high degree of alignment of (0002) lattice planes with (0001) substrate planes. Similar inferences were drawn from earlier ZnO epitaxial growth studies [5, 12], although much smaller FWHM ∼5 arc min was realized for ZnO epitaxy by plasma assisted MBE [3]. Simultaneous occurrence of the second peak in ω-rocking curve indicates that a portion of as-deposited ZnO film is

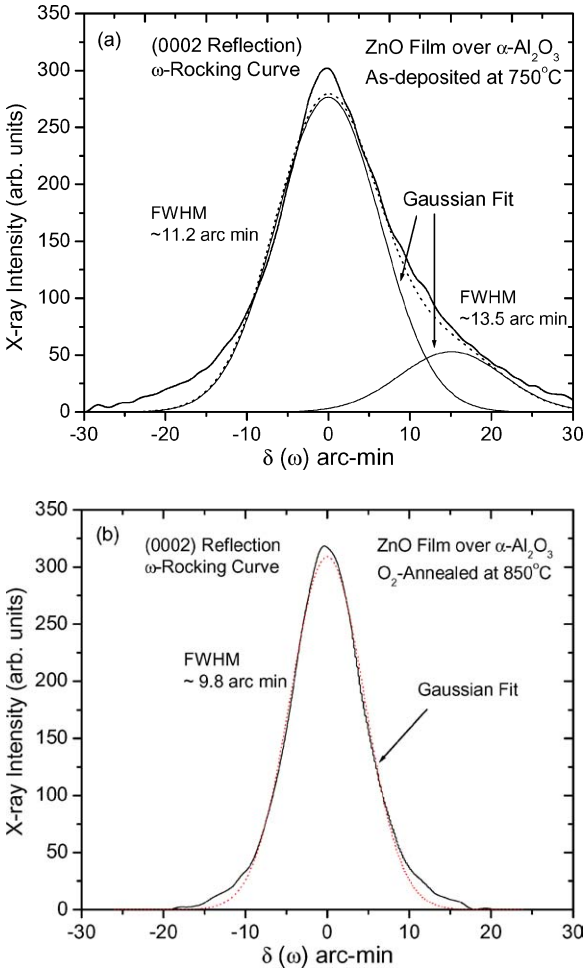

Fig. 3. (a) Rocking curve of (0002) reflection for as deposited ZnO film. Best fit Gaussian line profile fit with two separate peak features is shown by the dotted line. (b) Rocking curve of (0002) reflection for 850°C annealed ZnO film. Best fit Gaussian line profile for a single line with FWHM ∼9.8 arc min is shown by the dotted line.

oriented with different lattice plane-normal compared to bulk of film. Based on previous studies on ZnO films grown over imperfectly matched substrates [13, 14], it is inferred that differently oriented portion of ZnO film lies at the interface with Al_2O_3 substrate. Factors that might contribute to formation of such ZnO layer adjacent to substrate are directional defects. Defects such as screw dislocations with Burger vector parallel to *c*-axes in ZnO also cause crystallographic tilt in *c*-lattice planes and produce broadening of X-ray diffraction of (0002) in ZnO rocking curves [15, 16]. Asymmetric features of ω-rocking curves suggest that ZnO film growth by laser ablation occurs in two stages, an initial

ZnO layer characterized by directional lattice defects and subsequently formation of a highly crystalline ZnO layer. Substantial portion of ZnO film is having high degree of preferred *c*-axis orientation as seen from narrow and intense line profile. Thus, initially formed ZnO layer at interface is apparently a transition layer and subsequent ZnO growth gradually changes to attain much-improved *c*-axis oriented crystalline structure. Such two-layer growth behavior is likely to result in inclusion of strain in as-deposited ZnO films. Early growth can be regarded as highly strained growth mode and transition towards highly oriented ZnO film growth is accompanied by gradual relieving of strain. Lattice strain in as-deposited film is thus non-uniformly distributed in the direction perpendicular to (0002) plane [17, 18]. Further, analysis of line shapes of θ-2θ scans also indicates gradation in average depth concentration and strain in as-deposited ZnO films.

ZnO films after isothermal O_2-anneal at 850°C show ω-rocking curve having single high intensity peak with highly symmetrical line profile that is consistent with Gaussian curve as shown in Fig. 3(b). O_2-ambient annealing eliminated second broad asymmetric peak seen in ω rocking curves of as-deposited ZnO films. Second peak was associated with interfacial transition layer. Based on this layer, it was earlier inferred that as-deposited ZnO films could have strain with gradation in the direction of film growth. Emergence of single symmetrical line feature in O_2-annealed films appears to be result of structural changes in transition layer at the interface. This could in turn lead to reduction in elastic strain and its distribution along *c*-axis direction. O_2-annealed ZnO films show ω-rocking curve peak with FWHM ∼9.8 arc min reduced from 11.2 arc min seen in as-deposited films. This is close to lowest values reported for PLD grown ZnO films. Lower FWHM value also indicates reduction in lattice defects in annealed ZnO films. Annealing is generally known to remove certain defects and reduce stress in the films. However, this alone was not found sufficient for reduction in strain in ZnO films to the extent observed in this study. Annealing in O_2-ambient was found essential. Reduction in oxygen deficiency and as a result, compensation of oxygen vacancies and related defects in ZnO films after O_2 ambient annealing might have contribute towards decrease in strain.

It may be mentioned that oxygen vacancy defects are generally observed in ZnO films prepared by various growth techniques [19]. In PLD, availability of reactive oxygen through interaction with ZnO plasma in the plume created by focused laser beam is highly dependent on ambient pressure used for film growth. Present growth experiments were carried out at low oxygen pressure ∼1 mTorr and laser energy density ∼2–2.5 Joules/cm^2 at 10 Hz repeat rates. These conditions were used to prevent particulate formation and favor uniform ZnO flux at the substrate in order to form single crystal films, minimize defects, realize smooth surface morphology and achieve homogeneous growth. Such films are required for ZnO based optical devices. This deliberate choice of low oxygen pressure during growth of ZnO films might have further contributed to induction of O_2-vacancy defects.

3.2. *Electrical Resistivity*

ZnO films show *n*-type conduction as determined by sign of Hall-coefficient. Possible reason for this is formation of shallow donors associated with oxygen vacancies and interstitial Zn atoms [20]. Electrical resistivity of as deposited ZnO film is typically 0.3–0.8 ohm cm. Free carriers in ZnO originating from oxygen vacancies are possible cause of lower electrical resistivity [19, 21] Oxygen annealing of as-deposited ZnO films between 800–900°C increases electrical resistivity as shown by Fig. 4. This increase in resistivity by oxygenation is due to compensation of free carriers through reduction in oxygen vacancies [19, 21, 22].

3.3. *Photoluminescence Studies*

Optical properties of ZnO epitaxial films were investigated through PL measurements. Room temperature

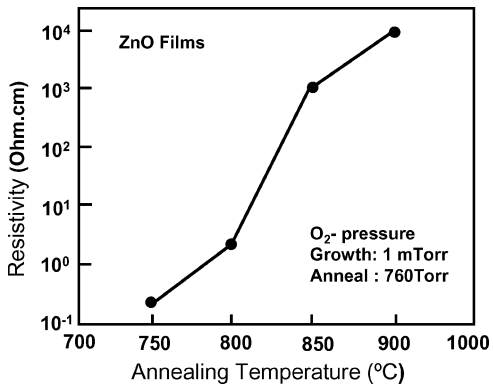

Fig. 4. Variation of electrical resistivity of ZnO films on O_2-annealing at different temperatures.

PL spectrum of ZnO epitaxial film grown on α-Al_2O_3 crystal is shown in Fig. 5(a). Prominent UV near band edge emission centered at 375.2 nm (3.302 eV) attributed to excitonic emission due to recombination of photo generated charge carriers dominates the spectrum. Features in UV emission band split by Gaussian fitting into two peaks are shown in Fig. 5(b). Dominant peak with narrow line width located at 374.6 nm (3.31 eV) is attributed to near band edge emission of bound neutral donors, $D^{\circ}X$ transition. Additional low intensity peak at 383.8 nm (3.23 eV) is due to complex defects and arises from electronic transition between donor-acceptor pairs [23]. UV emission peak shows a low energy tail, which is expected from localization of excitons in inhomogeneous strain fields, which is consistent with the observation of high compressive strains within ZnO films [24, 25]. A broad asymmetrical emission band observed in visible region is further separated into two broad peaks identified in Fig. 5(c) as, green-yellow emission bands at 498.0 nm (2.489 eV) and 527.5 nm (2.35 eV), respectively. Visible emission is not attributed to extrinsic impurities in ZnO, as X-ray photoelectron spectroscopy measurements have revealed no such impurities. Typically, visible emission in ZnO is caused by deep level defects. Relative intensity ratio of near band edge emission to visible emission $\sim$2.3 could be taken as an indication of high density of defects in the film. Biaxial strain in ZnO films affects only UV emission and causes no change in the position or intensity of deep level emission. According to θ-2θ diffraction and ω-rocking curve studies discussed earlier (Figs. 1–3), graded biaxial strain in laser ablation growth of ZnO thin films could be caused by transition of growth modes from an initial defect layer towards highly c-axis oriented defect free film on surface. ZnO films deposited at relatively higher O_2-partial pressures show increased intensity of UV emission (ratio $\sim$7–8). O_2-deficient ZnO film growth in early stages might contribute to both defects and gradation of strain along c-axis parallel to film growth direction.

Figure 6(a) shows PL spectrum of a ZnO film after O_2-annealing at 850°C. Significantly diminished intensity of deep level visible emission and corresponding increase in intensity of UV emission line (ratio $\sim$7.5) is attributed to reduction in oxygen vacancy defects. UV emission intensity of O_2 annealed ZnO films increases by $\sim$3.7 times in comparison to as-deposited ZnO films which is consistent with earlier inference of defect and strain reduction. Effect of strain reduction

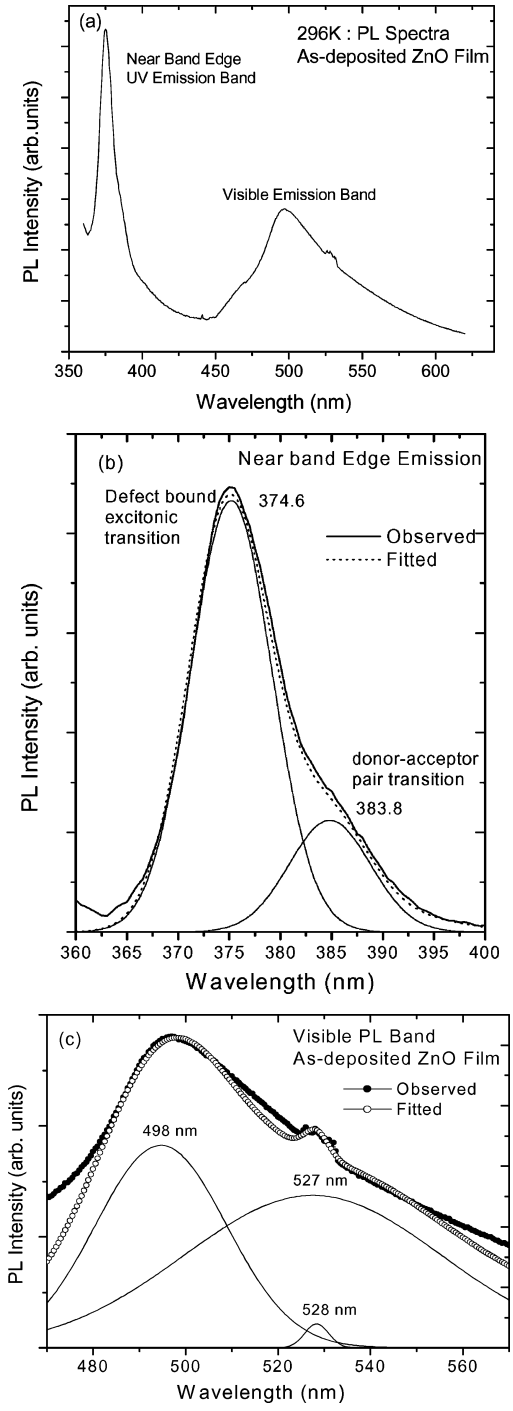

Fig. 5. (a) 296 K PL spectra of ZnO/α-Al_2O_3 structures formed by PLD grown 350 nm thick ZnO film in the as-deposited state showing near band edge UV and visible emission bands. (b) Fine structure of UV band by peak separation using Gaussian profile fit. (c) Fine structure of visible band separated as green and yellow emission peaks using Gaussian profile fit.

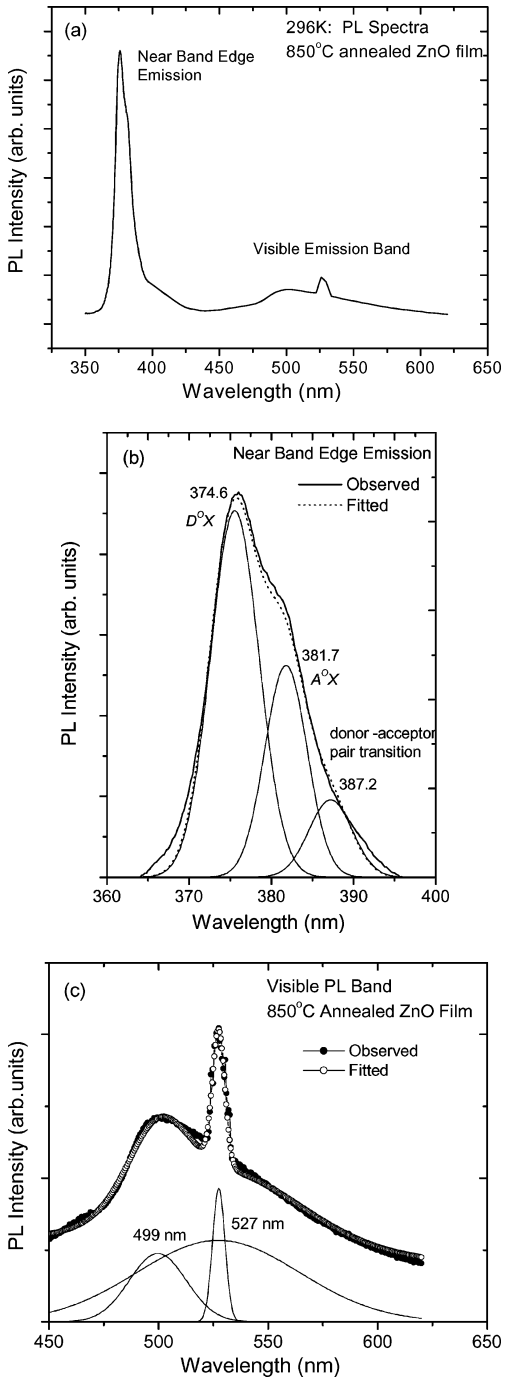

Fig. 6. (a) 296 K PL spectra of ZnO/α-Al_2O_3 structures formed by PLD grown 350 nm thick ZnO film after O_2-annelaing at 850°C showing near band edge UV and low intensity visible emission bands. (b) Fine structure of visible band separated as green and yellow emission peaks using Gaussian profile fit. (c) Fine structure of visible band separated as green and yellow emission peaks using Gaussian profile fit showing distinct yellow peak along with a broad peak.

on UV emission band is shown in Fig. 6(b). It is split into three peaks appearing at 374.6 nm (3.31 eV), 381.7 nm (3.25 eV) and 387.2 nm (3.20 eV). Transition energy for near band edge emission at 374.6 nm remains invariant. Peak initially located at 383.8 nm in strained ZnO film shifts towards lower energy and appears at 387.2 nm after annealing. Band structure calculations [24] show that with increased strain, excitonic transition energies shift towards higher energies. Displacement of transition energy of this excitonic peak by 28 meV towards lower energy side in annealed ZnO film is consistent with concurrent reduction in residual strain. O_2-annealed ZnO film shows a third emission peak of relatively high intensity and centered around 3.248 eV. In as- deposited ZnO films it is merged with near band edge. This near band edge peak is identified due to excitons bound to neutral acceptors $A^\circ X$ transitions. Observation of this emission peak became possible due to delocalization of exciton through minimization of strain inhomogenieties in O_2-annealed ZnO films. Intensity of $D^\circ X$ transitions is higher than $A^\circ X$ transitions due to n-type character of ZnO films. FWHM of near band edge emission line in PL spectra for as deposited and O_2-annealed ZnO films are 80 and 61 meV, respectively. Lowering of FWHM after annealing is in agreement with corresponding reduction in defects density and strain in annealed ZnO films. Consistent with the observation of lower FWHM of 9.5 arc min for ω-rocking curves, it is obvious that defect reduction, improvements in crystal quality and optical properties of ZnO epitaxial film occur simultaneously with O_2-annealing.

Analysis of visible emission band for O_2-annealed films is presented in Fig. 6(c). No substantive differences in positions of the two peaks, which comprise this emission band, are observed. However, reduction in intensity but a factor $\sim$4 compared to as-deposited films is caused by reduction in intrinsic defects. Relative intensity reduction of green over yellow broad emission is $\sim$1.5 times. In addition, a sharp emission line emerges at 527.5 nm (2.35 eV), which existed as a small peak in as-deposited ZnO films. Various mechanisms have been proposed to understand the origin of green-yellow PL emission in ZnO [26–30]. Vanheusden et al. [26] found that PL intensity of green emission at 2.495 eV in ZnO scales with increase in free electron carrier concentration and density of singly ionized oxygen vacancies $[V_o^+]$. Green emission arises by radiative recombination of electrons trapped at $[V_o^+]$ defect with photoexcited hole in valance band.

Considering that oxygen at high temperature rapidly diffuses into ZnO and recombines with O_2-vacancies, reduction in green emission intensity suggests that $[V_o^+]$ defects are responsible for green emission. Increase in resistivity of O_2-annealed ZnO films (Fig. 4) correlates well with oxygen vacancy defect mechanism. Yellow emission in ZnO arises from radiative optical transition in interstitial oxygen O_i [29]. Wu et al. [27] have shown that intensity of yellow emission increases in ZnO films deposited at higher O_2 pressures (increase in O_i) but decreases with increased deposition temperature (increase in V_o^+). O_2-annealing of ZnO films at higher (850°C) than growth temperature compensates for $[V_o^+]$ defects but at the same time may cause inclusion of O_i interstitials through $1/2\ O_2 = O_i$ dissociation. Thus, appearance of a sharp yellow emission peak and simultaneous reduction in green emission in annealed ZnO films could arise from O_i defects. Yellow emission band in Fig. 5(c) comprises of a sharp peak and a diffused band both centered on the same (2.35 eV) energy. This unusual structure of yellow band points out towards two different origins. According to Reynolds et al. [28], visible emission in ZnO is a result of transition between shallow donor with a deep acceptor complex involving Zn vacancy (V_{Zn}) defects. During high temperature O_2-annealing, V_{Zn} defects could form due to high diffusivity of Zn in ZnO compared to that of O_2 which supports out diffusion of Zn atoms into interstitial sites [26]. Following this yellow emission could also arise from V_{Zn} defects. We have no direct evidence which of the two, sharp and diffused yellow bands could be attributed to O_i or $[V_o^+]$, but since broad yellow band is present in as-deposited film in which O_i defects are unlikely, it is thought that broad yellow emission originates from V_{Zn} defects. Much smaller overall intensity of visible emission band relative to UV emission suggests that concentration of O_i and V_{Zn} defects formed by O_2-annealing is quite small as also evidenced from no adverse changes in the electrical properties. More perceptible effect of O_2-annealing lies in removal of oxygen vacancies, increased UV emission and relieving of graded compressive strain in ZnO films.

4. Conclusions

ZnO films over α-Al_2O_3 substrate with preferred c-axis orientation were deposited at 750°C under 1.0 mTorr O_2 background pressure by PLD technique. Deliberate choice of low O_2-pressure was dictated by need to form optical quality single crystal films for ZnO based optoelectronic device applications. ZnO film growth at higher O_2 pressure minimizes oxygen vacancies and thus could be more useful for devices and for p-conversion studies, but is also known to yield a rough surface morphology and often inclusion of additional defects such as low angle grain boundaries and interstitials [10]. ZnO films grown at low O_2-pressures show gradation of strain along the growth direction from interface region over substrate towards ZnO surface. Post deposition annealing in O_2 ambient at 850°C, higher than growth temperature, can compensate for O_2-vacancies and thus in reducing associated defects. Further, O_2 annealing causes lattice rearrangement resulting in relieving of inhomogeneous distribution of strain. Visible luminescence shows that smaller concentration of interstitial oxygen and zinc vacancy defect could arise without effecting electronic properties but can be avoided by appropriate choice of annealing parameters. Thus, optical quality ZnO films with high c-axis oriented crystal structure can be grown at relatively lower O_2-pressure without any adverse effects by combining the process with post growth higher temperature annealing in O_2-ambient.

Acknowledgments

We thank SHARP Laboratories Inc. of America and SHARP Microelectronics for sponsoring this project. This work was also supported in parts from DOE grant # DE-FG01-01ER45868 and NASA grant # NCC3-1034 which is gratefully acknowledged.

References

1. D.M. Bagnall, Y.F. Chen, Z. Zhu, T. Yao, M.Y. Shen, and T. Goto, *Appl. Phys. Letts.*, **73**, 1038 (1998).
2. D.M. Bagnall, Y.F. Chen, Z. Zhu, T. Yao, S. Koyama, M.Y. Shen, and T. Goto, *Appl. Phys. Letts.*, **70**, 2320 (1997).
3. H.J. Ko, Y.F. Chen, T. Yao, K. Miyajima, A. Yamamoto, and T. Goto, *Appl. Phys. Letts.*, **77**, 537 (2000).
4. S. Shrakata, K. Saeki, and T. Terasako, *J. Crystal Growth*, **237–239**, 528 (2002).
5. R.D. Vispute, V. Talyansky, Z. Trajanovic, S. Choopun, M. Downes, R.P. Sharma, M. Venkatesan, M.C. Woods, R.T. Lareau, K.A. Jones, and A.A. Iliadis, *Appl. Phys. Lett.*, **70**, 2735 (1997).
6. V. Cracium, J. Perriere, N. Basim, R.K. Singh, D. Cracium, and J. Spear, *Appl. Phys. A.: Mater. Sci. Process.*, A **69**, S531 (1999).

7. A. Ohmoto, M. Kawasaki, T. Koida, K. Masubuchi, H. Koinuma, Y. Sakurai, Y. Yoshida, and Y. Segawa, *Appl. Phys. Letts.*, **76**, 550 (1998).
8. K. Sakurai, M. Kanehiro, K.K. Nakahara, T. Tanabe, S. Fijita, and S. Fujita, *J. Crystal Growth*, **209**, 522 (2000).
9. S-H. Lim, D. Shindo, H.-B. Kang, and K. Nakamuara, *J. Vac. Sci. Technol. B*, **19**, 506 (2001).
10. I.C. Noyan, T.C. Huang, and B.R. York, *Crit. Rev. in Solid State and Mat. Sci.*, **20**, 125 (1995).
11. W. Shan, R.J. Heuenstein, A.J. Fischer, J.J. Song, W.G. Perry, M.D. Bremser, R.F. Davis, and B. Goldenberg, *Phys. Rev. B*, **54**, 13460 (1996).
12. J. Narayan, K. Dovidenko, A.K. Sharma, and S. Oktyabrsky, *J. Appl. Phys.* **84**, 2597 (1998).
13. V. Cracium, J. Elders, J.G.E. Gardeniers, and I.W. Boyd, *Appl. Phys. Lett.*, **65**, 2963 (1994).
14. E. Vasco, J.R. Zuazo, L. Vazquez, C. Prieto, and C. Zaldo, *J. Vac. Sci. Technol. B*, **19**, 224 (2001).
15. B. Heying, X. Wu, S. Keller, Y. Li, D. Kapolnek, B.P. Keller, S.P. DenBaars, and J.S. Speck, *Appl. Phys. Lett.*, **68**, 643 (1996).
16. Q. Zhu, A. Botchkarev, W. Kim, O. Akas, A. Salvador, B. Sverdlov, H. Morkoc, S.-C.Y. Tsen, and D.J. Smith, *Appl. Phys. Lett.*, **68**, 1141 (1999).
17. Y.F. Chen, D.M. Bagnall, H.J. Ko, K.T. Park, K. Hiraga, Z. Zhu, and T. Yao, *J. Appl. Phys.*, **84**, 3912 (1998).
18. H.J. Ko, Y.F. Chen, Z. Zhu, T. Hananda, and T. Yao, *J. Crystal Growth*, **208**, 389 (1999).
19. Z.M. Jarzebski, in *Oxide Semiconductors*, edited by B. Grzybowska-Swierkosz and B.R. Pamplin (Pergamon, Oxford, 1973) Chap. 13, p. 228.
20. A.F. Kohan, G. Ceder, D. Morgan, and Chris G. Van de Walle, *Phys. Rev. B*, **61**, 15019 (2000).
21. S. Choopan, R.D. Vispute, W. Noch, A. Balsamo, R.P. Sharma, T. Venkatesan, A. Illiadis, and D.C. Look, *Appl. Phys. Lett.*, **75**, 3947 (1999).
22. T. Minami, H. Nanto, and S. Takata, *Jpn. J. Appl. Phys.*, **23**, L280 (1984).
23. R.D. Vispute, V. Talyansky, S. Choopun, R.P. Sharma, T. Venkatesan, M. He, X. Tang, J.B. Halpern, M.G. Spencer, Y.X. Li, L.G. Salamanca-Riba, K.A. Jones, and A.A. Iliadis, *Appl. Phys. Lett.*, **73**, 348 (1998).
24. H.C. Ong, A.X.E. Zhu, and G.T. Du, *Appl. Phys. Lett.*, **80**, 941 (2002).
25. V. Srikant and D.R. Clarke, *J. Appl. Phys.*, **81**, 6357 (1997).
26. K. Vanheusden, W.L. Warren, C.H. Seager, D.R. Tallant, J.A. Voigt, and B.E. Gnade, *J. Appl. Phys.*, **79**, 7983 (1996).
27. X.L. Wu, G.G. Siu, C.L. Fu, and H.C. Ong, *Appl. Phys. Lett.*, **78**, 2285 (2001).
28. D.C. Reynold, D.C. Look, B. Jogai, J.E. Van Nostrand, R. Jones, and J. Jenny, *Sol. Stat. Comm.*, **106**, 701 (1998).
29. M. Liu, A.H. Kitai, and P. Mascher, *J. Lumin.*, **54**, 35 (1992).
30. H.Y. Lee, H.J. Ko, and T. Yao, *Appl. Phys. Lett.*, **82**, 523 (2003).